Electrical Power and Energy Systems 107 (2019) 379–394

Contents lists available at ScienceDirect

Electrical Power and Energy Systems

journal homepage: www.elsevier.com/locate/ijepes

A novel data-driven approach for transient stability prediction of power systems considering the operational variability

Yanzhen Zhou[a], Qinglai Guo[a], Hongbin Sun[a,*], Zhihong Yu[b], Junyong Wu[c], Liangliang Hao[c]

[a] Department of Electrical Engineering, State Key Laboratory of Electricity Systems, Tsinghua University, 100084 Beijing, China
[b] China Electric Power Research Institute, 100192 Beijing, China
[c] School of Electrical Engineering, Beijing Jiaotong University, 100044 Beijing, China

ARTICLE INFO

Keywords:
Data driven
Transient stability prediction
Convolutional neural network
Active learning
Fine-tuning

ABSTRACT

Data driven methods are playing an increasingly important role in transient stability assessment, primarily because of the availability of large annotated datasets. Nevertheless, training data cannot cover all the possible operating conditions of a modern power system with variable power generations and loads. The classifier should adjust to the near-future operation condition in limited time, and this adjustment may be hindered by the computational time of the simulations and classifier training. To dramatically reduce the computational cost, this paper presents a systematic approach for building and updating an accurate transient stability classifier. First, the time-series trajectories of generators after disturbance are used as the inputs, and then a convolutional neural network (CNN) ensemble method is proposed to generate the transient stability predictor using these multi-dimensional data. To reduce the misclassification of instability, different cost weights are considered for the stable and unstable instances in the loss function. When the operating condition changes substantially and makes the pre-trained classifier unavailable, the active learning and fine-tuning techniques are integrated to update the classifier with good performance using fewer labelled instances and short computational time. The simulation results of two power systems illustrate the effectiveness of the proposed approach.

1. Introduction

During the past several years, there has been a substantial promotion of renewable energy and flexible loads to modern power systems, which brings challenges for the security and stability of the power system [1]. Transient stability, or large-disturbance rotor angle stability, is one of the major concerns for planning, operation and control of power systems [2]. Many dynamic units in power systems act on one another, which results in the complexity of transient stability analysis.

The most accurate method for transient stability analysis is time-domain simulation; however, this approach is time consuming, especially for large-scale power systems. In [3], the piecewise constant-current load equivalent is proposed to reduce the computing time for integrating the differential/algebraic equation model of post-fault power system dynamics, but the computational speed seems insufficient for real-time application. By contrast, the direct methods, such as transient energy function method [4] and extended equal-area criterion [5], can compute quickly and provide the stability margin, whereas the model limitations are inevitable. In [6], a hybrid method based on the new concept of equal area criterion and corrected kinetic energy function is proposed for real-time transient stability assessment. It can be concluded that the methods with detailed models can provide accurate prediction, whereas the computation speed seems insufficient for real-time application. To achieve the fast prediction, it is unavoidable to make some assumptions to simplify the problem at the expense of accuracy.

Thanks to the wide availability of massive energy data in the power systems, it is expected that data analytics will play an increasingly important role in modern power systems [7,8]. Data-driven method, which has powerful and flexible modelling capability [9], as well as the fast prediction after the inputs are obtained, has been considered as alternatives for transient stability prediction [10–17].

When using the data-driven methods for transient stability prediction, a set of appropriate features should be selected and extracted as the inputs; then an appropriate classification method is utilized to predict the transient stability status. The input features of data-driven based methods used for transient stability prediction include the generator rotor angles and speeds [10–13], generator terminal voltages [14,15], apparent impedance [16] and the combination of different variables [17], etc. In [18], the terms of transient energy functions are

[*] Corresponding author.
E-mail address: shb@tsinghua.edu.cn (H. Sun).

https://doi.org/10.1016/j.ijepes.2018.11.031
Received 27 June 2018; Received in revised form 24 October 2018; Accepted 26 November 2018

used as the input features. In [19], several wide-area severity indices are defined in the time and frequency domains. These indices are used as the inputs to build the classifiers for catastrophe predictor. In [20], the empirical orthogonal function is used for feature extraction and selection before training a classifier for transient stability analysis.

Various algorithms have been used to train the classifier for transient stability prediction, such as artificial neural network [10], decision tree [11–14,16,21], support vector machine [15,17,18,20,22], and random forest [19]. Recently, the rapid development of deep learning has promoted the widespread exploration of deep learning in industry applications [23–28]. The deep learning model can provide more accurate results than the shallow models. In [29], the long short-term memory (LSTM) is proposed for transient stability prediction. The results show that the LSTM-based method can achieve a superior assessment accuracy within a short period of time after disturbance.

In general, there are two types of application scenarios for the data-driven based methods. One scenario is to analyse the transient stability considering anticipated but non-occurring contingencies [18,30]. In this case, the steady-state measurements are usually used as the inputs [30]. When the power system is predicted as insecure, prevention control actions should be conducted. In [18], the post-disturbance data are used for online dynamic security assessment considering anticipated contingencies. These dynamic data can be obtained from short-term simulations and the generated classifier has good performance. Therefore, the dynamic data can also be used for pre-contingency analysis. The other scenario is to provide real-time prediction of the transient stability status after contingences [10–17,19,20]. In this case, the dynamic responses of different variables that can be obtained by wide area measurement systems are always used as the inputs.

This paper focuses on the transient stability prediction using dynamic data. The dynamic data can be obtained from post-contingency real-time measurements or pre-contingency short-term simulations. Therefore, the proposed method can be applied to predict the transient stability status under both occurred and anticipated contingencies. When using the dynamic trajectories of different variables and different generators for transient stability prediction, the input is a massive amount of spatio-temporal data. Spatio-temporal data can be stored as multi-dimensional arrays and have similar data structure to that of the images. This characteristic motivated us to utilize the convolutional neural network (CNN) [31], a popular deep learning network especially in computer vision applications, to perform the transient stability prediction. During the operation of power systems, the operating conditions, such as the load levels and network topologies, vary with generation and load changes, generation dispatch, scheduled maintenance, etc. Thus, the number of possible operating conditions is infinite, and there are unavoidable differences between the offline training and the practical conditions. The classifier obtained by offline simulation and historical data may become unsuitable and need to be updated periodically [18,19,21]. To obtain a new classifier, a comprehensive dataset should be generated considering the uncertainties associated with load levels, system topology, fault types, locations, clearance time, etc. And the classifier is retrained using the new dataset. The data generation and classifier retraining may be time consuming and become an obstacle for updating.

To dramatically reduce the computational cost of classifier updating, this paper presents a CNN-based method integrating active learning and fine-tuning techniques. Active learning aims to train an accurate model with low cost by only labelling the important instances [32,33]. Fine-tuning involves adapting an existing pre-trained model to another domain by executing a few training iterations on a new dataset [23]. By integrating these two techniques, the generated classifier can be updated using less training instances in shorter time, making the updating process more suitable for practical application.

The main contributions of this paper can be summarized as follows: (1) All the time-series features are stored as multi-dimensional arrays, and then three different CNNs with different window sizes of kernels are built to construct an ensemble classifier with high accuracy and generalization ability. (2) Before the operating conditions and topologies change greatly (as predicted by generation and load forecasting, dispatching, scheduled maintenance, etc.), the classifiers can be updated rapidly by fine-tuning the pre-trained classifier using the most informative and representative instances, and the computational costs of both the data generation and classifier training process are greatly reduced, making the proposed approach more suitable for practical application.

The remainder of this paper is organized as follows. The physical description of transient stability, the mathematical description and analysis of data-driven based method for transient stability analysis are included in Section 2. Section 3 introduces the proposed CNN ensemble classifier considering the high-dimensional characteristic of the inputs. The total data-driven approach for transient stability prediction considering the operational variability is described in Section 4. Comprehensive case studies and discussions are presented in Section 5. The conclusions are given in Section 6.

2. Problem description and analysis

The basic structure of power system for transient stability analysis is shown in Fig. 1.

There is one synchronous generator combined with the loads and other dynamic units through the power grid. The imbalance between the generator mechanic power P_m and electromagnetic power P_e is associated with the variation of rotor angles and speeds. The rotor speed signal is then put into the prime mover and its speed control system to control the output torque of the prime mover T_m, and hence influence the P_m. On the other hand, the generator voltage U_t is echoed back to the excitation system to control the field voltage E_f. For practical power systems, there are many generators, loads and other dynamic units. These units are combined together through the power grid and act on one another, which results in the complexity of transient stability analysis.

Data driven methods have been adopted as alternative approaches for transient stability analysis, which is mainly because the rapid computation. When using data driven methods to predict the transient stability, a set of variables $\boldsymbol{X}_i = (\boldsymbol{X}_{i,1}, \boldsymbol{X}_{i,2},\ldots, \boldsymbol{X}_{i,k})$ should be selected to describe the operating conditions of power systems. Next, a set of

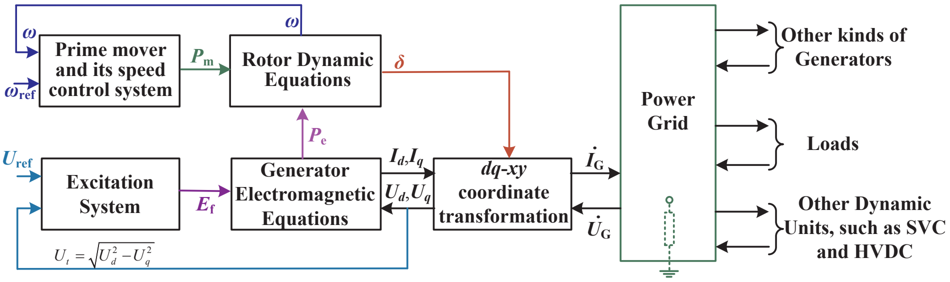

Fig. 1. Basic structure of power system model for transient stability analysis [34].

Table 1
Descriptions of different input features.

Input features	Descriptions
Relative rotor angle [5] of generator i at $t = t_k$	$\widetilde{\delta}_i(t_k) = \delta_i(t_k) - \sum_{i=1}^{n} M_i\delta_i(t_k)/\sum_{i=1}^{n} M_i$
Relative rotor speed of generator i at $t = t_k$	$\widetilde{\omega}_i(t_k) = [\widetilde{\delta}_i(t_k) - \widetilde{\delta}_i(t_{k-1})]/\Delta t$
Relative rotor acceleration of generator i at $t = t_k$	$\widetilde{\alpha}_i(t_k) = [\widetilde{\delta}_i(t_k) - \widetilde{\delta}_i(t_{k-1}) + 2\widetilde{\delta}_i(t_{k-2})]/\Delta t$
Kinetic energy of generator i at $t = t_k$	$EK_i(t_k) = \frac{1}{2}M_i(\widetilde{\omega}_i(t_k))^2$
Relative electromagnetic power of generator i at $t = t_k$	$\widetilde{P}_{ei}(t_k) = P_{ei}(t_k)/P_{ei}(0_-)$

where n is the total number of generators, M_i is the inertia coefficient of generator i, $\delta_i(t_k)$ is the rotor angle of generator i at $t = t_k$, $\Delta t = t_k - t_{k-1} = t_{k_{-1}} - t_{k-2}$, $P_{ei}(t_k)$ is the electromagnetic power of generator i at $t = t_k$.

instance-label pairs ($\boldsymbol{X}_i$,y_i) is obtained considering different load levels, network configurations and contingencies by simulation or historical measurements. By training from massive data, the data-driven method can find a mapping between the input features $\boldsymbol{X}_i$ and the transient stability analysis result y_i: $\psi(\boldsymbol{X}_i) = y_i$.

The transient stability directly depends on the dynamics of generator rotor angles. Thus, the rotor angle-related variables are always used as the inputs [10–13,17]. Moreover, the rotor angle is affected by the electromagnetic power [17]. When the fault occurs, the electromagnetic power will suddenly change. After the fault clearance, relative electromagnetic power of the i-th generator, $P_{ei}(t)/P_{ei}(0\text{-})$, reflects the recovery of the electromagnetic power. In this research, the dynamic trajectories of the relative rotor angles, the speeds, the accelerations, the kinetic energy, and the relative electromagnetic power of all the generators are used as the inputs. Detail information of the input features are shown in Table 1. More case studies and discussions about the input features will be provided in Section 5.3 and 5.6.

The aforementioned input data can be stored as multi-dimensional arrays, as shown in Fig. 2.

The input data are high dimensional when using these time-series features, especially for a large-scale power system with hundreds of generators. As a result, the computational space and time increase greatly with increasing system size. Actually, the data structure of these time-series variables is similar to that of the images. The variable axis of these time-series data depicts different views of all the generators (e.g., the rotor angle, speed, kinetic energies), analogous to the colour channels of an image. Moreover, there are two axes (time and generator) featuring different variables that can be viewed as being analogous to the width and height axes of the image. This characteristic motivated us to utilize the CNN, a well-known deep learning method for image classification, to perform the transient stability prediction using these time-series features.

3. CNN ensemble classifier for transient stability prediction

3.1. Brief introduction of CNN

For the transient stability prediction with high-dimensional input, it is not practical to apply the fully connected neural network to generate a classifier since a high number of weights for each neuron is necessary. And the required number of training instances will increase as the parameter number increases. The CNN provides a solution to reduce the parameter number. The convolutional neuron shares the same weights to each spatial location (i,j); therefore, the parameter number is greatly reduced. The output $o_{i,j}$ of a convolutional layer with location (i, j) is as follows:

$$o_{i,j} = \sigma((\boldsymbol{W} \otimes \boldsymbol{X})_{i,j} + b) \tag{1}$$

where $\boldsymbol{W}$ is a kernel with learned weight, b is the bias, "⊗" is the convolution operation that is always substituted by the correlation operation, and $\sigma()$ is the activation function. After the convolutional layer, it is common to add a pooling layer to reduce the data dimension. The most commonly used pooling layer, max-pooling, is utilized here.

After the convolutional and pooling process, an activation layer is required to make the learned features more dividable. In this research, the activation function of the convolutional layers and the pooling layers is the rectified linear unit (ReLU), which is widely used as an activation unit to accelerate the convergence of the CNN [31]:

$$ReLU(x) = \max(0, x) \tag{2}$$

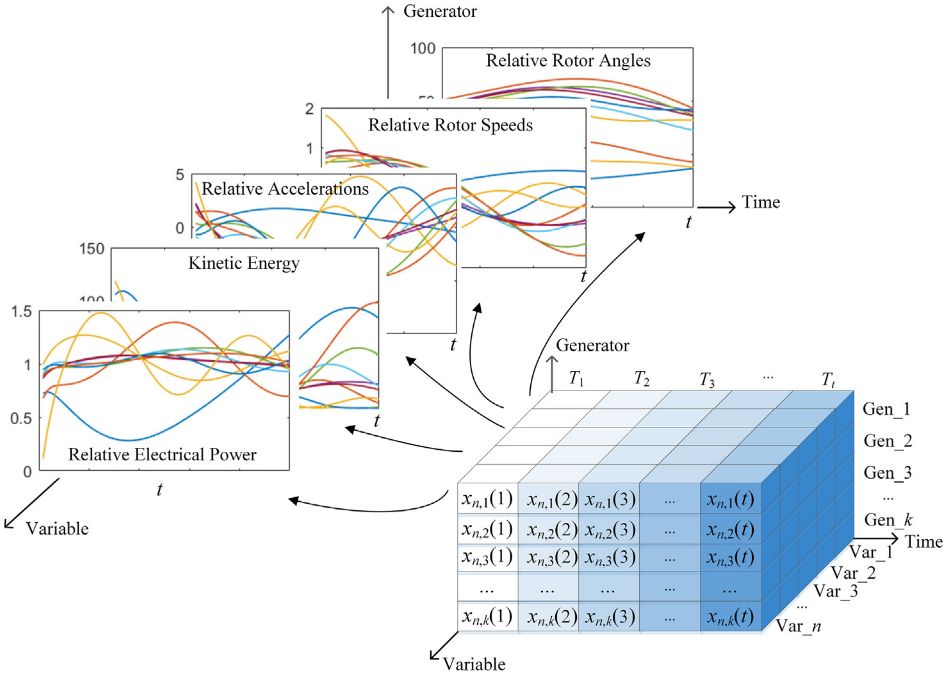
Generator
100
Relative Rotor Angles
2
1
Relative Rotor Speeds
5
0
Relative Accelerations
150
100
Kinetic Energy
1.5
1
0.5
0
Relative Electrical Power
t
Variable
Time
Generator
T_1 T_2 T_3 ... T_t
Gen_1
Gen_2
Gen_3
...
Gen_k
Time
$x_{n,1}(1)$ $x_{n,1}(2)$ $x_{n,1}(3)$ ... $x_{n,1}(t)$
$x_{n,2}(1)$ $x_{n,2}(2)$ $x_{n,2}(3)$ ... $x_{n,2}(t)$
$x_{n,3}(1)$ $x_{n,3}(2)$ $x_{n,3}(3)$ ... $x_{n,3}(t)$
... ...
$x_{n,k}(1)$ $x_{n,k}(2)$ $x_{n,k}(3)$ ... $x_{n,k}(t)$
Var_1
Var_2
Var_3
...
Var_n
Variable

Fig. 2. Data structure of the time-series variables for transient stability prediction.

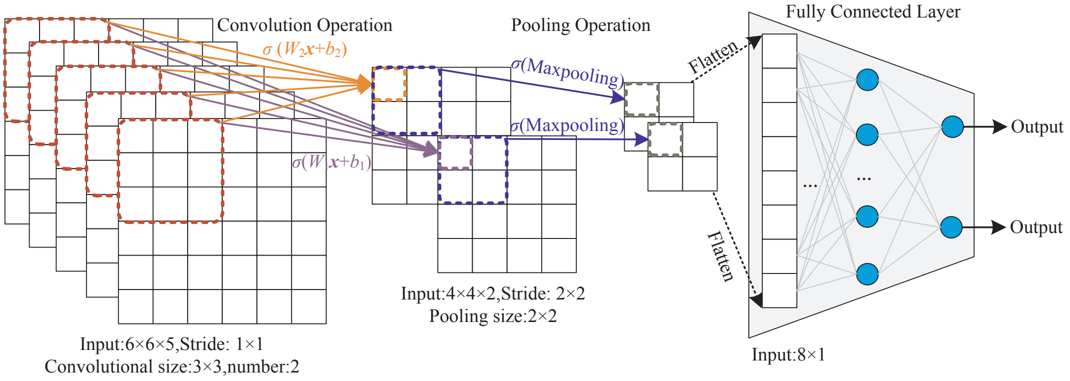

Fig. 3. Basic structure of CNN with one convolution and pooling layer.

where x is the input to the activation layer.

A fully connected layer is required to generate the classification stage after the convolutional layers and pooling layers. The mathematical representation of fully-connected layer is:

$$o_{i,j} = \sigma_2(\boldsymbol{W}_f * \boldsymbol{X}_f + b_f) \tag{3}$$

where $\boldsymbol{X}_f$ is the input data of the fully-connected layer, $\boldsymbol{W}_f$ is the weight matrix, b_f is the bias. The activation function of the fully connected layer is Softmax:

$$P(C_k|\boldsymbol{X}) = \frac{e^{V_k(\boldsymbol{X})}}{\sum_{k=1}^{2} e^{V_k(\boldsymbol{X})}} \tag{4}$$

where $V_k(\boldsymbol{X})$ is the k-th input data of the Softmax layer with instance $\boldsymbol{X}$, $P(C_1|\boldsymbol{X})$ and $P(C_2|\boldsymbol{X})$ are the probabilities of an unknown instance $\boldsymbol{X}$ identified as class-1 and class-2 (binary classification), respectively. The final output of CNN is $\hat{\boldsymbol{y}}_i = (\hat{y}_i^{(1)},\ \hat{y}_i^{(2)}) = (P(C_1|\boldsymbol{X}),\ P(C_2|\boldsymbol{X}))$. If $P(C_1|\boldsymbol{X}) > P(C_2|\boldsymbol{X})$, then the unknown instance will be identified as class 1 and vice versa.

Fig. 3 shows a CNN structure with one convolution and pooling layer.

The weight matrix and the corresponding biases in CNN are achieved through the minimization of the loss between the true label vectors $\boldsymbol{y}_i = (y_i^{(1)},\ y_i^{(2)})$ and the predicted label vectors $\hat{y}_i = (\hat{y}_i^{(1)},\ \hat{y}_i^{(2)})$, for N training instances $i = 1,\ldots,N$. If $y_i^{(1)} = 1$, then the unknown instance will be identified as stable and vice versa. In this research, the common cross-entropy loss is used as the loss function, shown as Eq. (5)

$$L = -\frac{1}{N}\sum_{i=1}^{N} H(\boldsymbol{y}_i, \hat{\boldsymbol{y}}_i) = -\frac{1}{N}\sum_{i=1}^{N} [y_i^{(1)}\log(\hat{y}_i^{(1)}) + y_i^{(2)}\log(\hat{y}_i^{(2)})] \tag{5}$$

where N is the total number of training instances. The cross-entropy loss has fast convergence rates and is numerically stable when coupled with softmax normalization [35].

The Adam stochastic optimization algorithm is applied to minimize the loss function. Adam is a straightforward, memory-saving and computationally effective method and is quite suitable for models with large inputs of data. Details of this optimization algorithm can be found in [36].

3.2. Proposed CNN-based ensemble classifier

For the transient stability prediction, the original training data are always unbalanced with fewer unstable instances. This condition will lead to under-fitting for unstable instances. If a stable case is false alarmed, then there is little impact on the power system security because the emergency measures always make the power system strong. In contrast, an unstable case that is misidentified will result in a disaster when no measure has been taken to prevent the collapse. Therefore, the cost of misdetecting instability is greater than stability. One solution to reduce the misdetection of instability is to set different costs to impose greater weight on the unstable instances, and the loss function in Eq. (5) can be rewritten as

$$L = -\frac{1}{N}\sum_{i=1}^{N} [W_s y_i^{(1)}\log(\hat{y}_i^{(1)}) + W_{us} y_i^{(2)}\log(\hat{y}_i^{(2)})] \tag{6}$$

where W_{us} and W_s are the cost weight of unstable and stable instances, respectively. When $W_{us} = W_s = 1$, the loss function put the same importance to the stability and instability. When $W_{us} > W_s$, that means the misdetection cost of instability is greater than stability.

On the other hand, the performance of a CNN is greatly influenced by the parameter construction. In the literatures, the window sizes of the first convolutional layer of different kinds of CNNs are different, e.g., 3 × 3 [37], 5 × 5 [31] and 7 × 7 [38]. The size of the first convolutional layer can be larger than that of the subsequent layers, but a larger window size corresponds to more parameters. The most commonly used size of the other convolutional layers is 3 × 3, and the size of max-pooling is usually selected as 2 × 2 [31,37,38]. A better classifier with appropriate construction can only be determined via many time-consuming trials. Moreover, it is difficult to ensure that the selected classifier can always perform the best of any test scenarios. For this reason, different CNNs with different parameter configurations are trained to construct an ensemble classifier. All the sub-classifiers can be trained by multiple graphic processing units (GPUs), making the proposed approach more suitable for practical application. It should be noted that the determination of CNN number should depend on the comprehensive case studies and hardware condition. The combination of different classifiers is a successful approach to reduce test errors [39]. Whereas, using too many CNNs may require more graphic processing units. In this research, three different CNNs are trained to generate the ensemble classifier to verify the effectiveness. For different applications and hardware conditions, the number of CNNs may be different.

Two types of power systems are used for case studies: the New England 10-machine 39-bus system and the Northeast Power Coordinating Council (NPCC) 48-machine 140-bus system. It is assumed that all the dynamic variables are sampled simultaneously every cycle (0.0167 s for 60 Hz system), therefore the input features are time series of which time interval is 0.0167 s. The response time of dynamic trajectories is $N_{\text{cycle}}/60$ s in the case studies; so, the number of cycles is N_{cycle}. The input sizes are $N_{\text{cycle}} \times 10 \times 5$ and $N_{\text{cycle}} \times 48 \times 5$ for the 10-machine and 48-machine test systems, respectively. Two convolutional and max pooling layers are enough for these two kinds of data. The data pre-processing and network structure of proposed CNN ensemble classifier are shown in Fig. 4.

In Fig. 4, all the input data are pre-processed by maximum and minimum normalization first. Then, the normalized data are divided into three axes according to the generator number, variables and response time. Therefore, the input size are $N_{\text{cycle}} \times 10 \times 5$ and $N_{\text{cycle}} \times 48 \times 5$ for the 10-machine system and the 48-machine system,

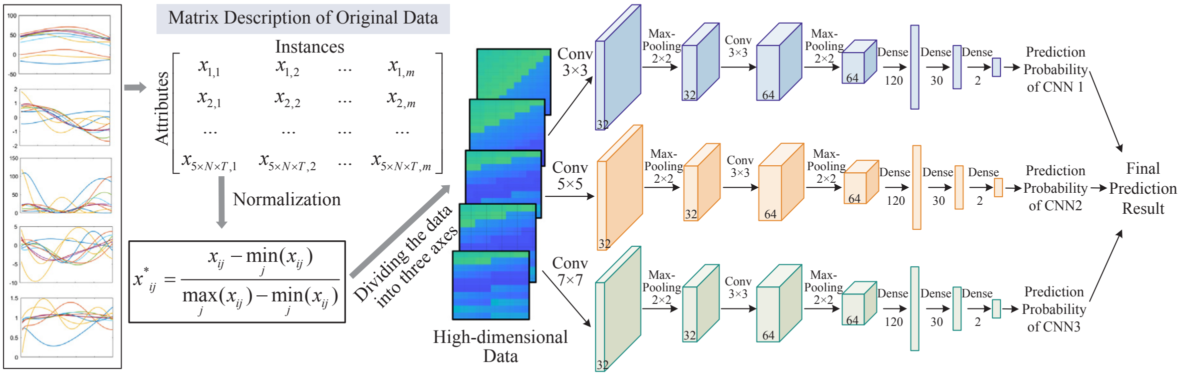
Matrix Description of Original Data
Instances
Attributes
$x_{1,1}$ $x_{1,2}$ … $x_{1,m}$
$x_{2,1}$ $x_{2,2}$ … $x_{2,m}$
$x_{5\times N\times T,1}$ $x_{5\times N\times T,2}$ … $x_{5\times N\times T,m}$
Normalization
$x^*_{ij} = \frac{x_{ij} - \min_j(x_{ij})}{\max_j(x_{ij}) - \min_j(x_{ij})}$
Dividing the data into three axes
High-dimensional Data
Conv 3×3
Conv 5×5
Conv 7×7
Max-Pooling 2×2
Dense
32
64
120
30
2
Prediction Probability of CNN 1
Prediction Probability of CNN2
Prediction Probability of CNN3
Final Prediction Result

Fig. 4. The data pre-processing and network structure of the proposed CNN-based ensemble classifier.

Table 2
Details of the CNN models.

Layer	Kernel Size/Stride		Kernel Number	Padding	Output size	
	10-machine	48-machine			10-machine	48-machine
1. Convolution	(1) 3 × 3/1 × 1 (2) 5 × 5/1 × 1 (3) 7 × 7/1 × 1	(1) 3 × 3/1 × 2 (2) 5 × 5/1 × 2 (3) 7 × 7/1 × 2	32	Same	$N_{\text{cycle}} \times 10 \times 32$	$N_{\text{cycle}} \times 24 \times 32$
2. Pooling	2 × 2/2 × 2	2 × 2/2 × 2	32	Same	$\lceil N_{\text{cycle}}/2\rceil \times 5 \times 32$	$\lceil N_{\text{cycle}}/2\rceil \times 12 \times 32$
3. Convolution	3 × 3/1 × 1	3 × 3/1 × 2	64	Same	$\lceil N_{\text{cycle}}/2\rceil \times 5 \times 64$	$\lceil N_{\text{cycle}}/2\rceil \times 6 \times 64$
4. Pooling	2 × 2/2 × 2	2 × 2/2 × 2	64	Same	$\lceil N_{\text{cycle}}/4\rceil \times 3 \times 64$	$\lceil N_{\text{cycle}}/4\rceil \times 3 \times 64$
5. Fully connected	120	120	1	–	120 × 1	120 × 1
6. Fully connected	30	30	1	–	30 × 1	30 × 1
7. Softmax	2	2	1	–	2	2

respectively. These high-dimensional data are placed into three different CNNs with two convolutional and max pooling layers, two fully connected hidden layers and a Softmax layer at the end. The activation function of convolutional layers and pooling layers is ReLU. The window sizes of the first convolutional layer of the three CNNs are 3 × 3, 5 × 5 and 7 × 7 respectively. The detail parameters of the CNN classifiers are shown in Table 2.

Moreover, dropout [40,41] is used in the fully connected layers of Fig. 4. The neuron in the l-th fully connected layer after dropout is as follows:

$$\begin{cases} r_j^{(l)} \sim Bernoulli(p) \\ y_i^{(l+1)} = \sigma(\boldsymbol{w}_i^{(l+1)}(\boldsymbol{r}^{(l)}\boldsymbol{y}^{(l)}) + b) \end{cases} \tag{7}$$

where $\boldsymbol{r}^{(l)}$ is a vector of independent Bernoulli random variables, each of which has probability p of being 1 [41]; $\boldsymbol{y}^{(l)}$ is the input vector of the dropout layer; and $\boldsymbol{y}^{(l+1)}$ is the output after dropout. The final output of the ensemble classifier is the average of all the CNNs' probabilistic outputs:

$$P_z(C_k|\boldsymbol{X}) = \frac{\sum_{s=1}^{3} P_s(C_k|\boldsymbol{X})}{3} \tag{8}$$

where $P_s(C_k|\boldsymbol{X})$ is the probabilities of class k with respect to an unknown instance $\boldsymbol{X}$ using the s-th CNN. Similar with the definition of confidence in [43], the prediction confidence of CNN ensemble classifier is $CIz = \max\{P_Z(C_1|\boldsymbol{X}), P_Z(C_2|\boldsymbol{X})\}$.

4. Data-driven approach for transient stability prediction considering the operational variability

The data-driven method for transient stability prediction consists of three important processes: (1) Offline classifier training, (2) Period updating and (3) Practical application. The temporal relationships of these three processes are shown in Fig. 5.

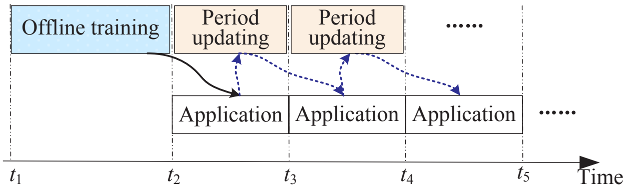

Fig. 5. Temporal relationships of three important processes.

The offline training and period updating process should be finished before application. Detail of the data-driven method for transient stability prediction is shown in Fig. 6.

4.1. Offline classifier training

During the offline training process, a comprehensive dataset, $(\boldsymbol{X}_i, y_i)$, should be generated for the next application period (e.g. t_2-t_5 in Fig. 5), where $\boldsymbol{X}_i = (\boldsymbol{X}_{i,1}, \boldsymbol{X}_{i,2}, \ldots, \boldsymbol{X}_{i,k})$ is a set of input variables, y_i is the transient stability status of the i-th instances based on long-term time-domain simulation, $i = N_{\text{oc}} \times N_{\text{c}}$ represents that N_{oc} operation conditions (OCs) and N_{c} contingencies are included in the dataset, the determination of N_{oc} and N_{c} is related to the scale of power systems and the time period for application. The uncertainties associated with load levels, system topology, fault types, locations, clearance time should be considered [11]. By training from massive data, the data-driven method can find a mapping between the input features $\boldsymbol{X}_i$ and the transient stability analysis result y_i: $\psi(\boldsymbol{X}_i) = y_i$. Before application, the classifier should be verified by several test datasets or cross-validation to avoid the over-fitting.

4.2. Period updating integrating active learning and Fine-tuning techniques

The updating process should be conducted infrequently on daily, hourly or shorter. The prospective OCs in the next period can be

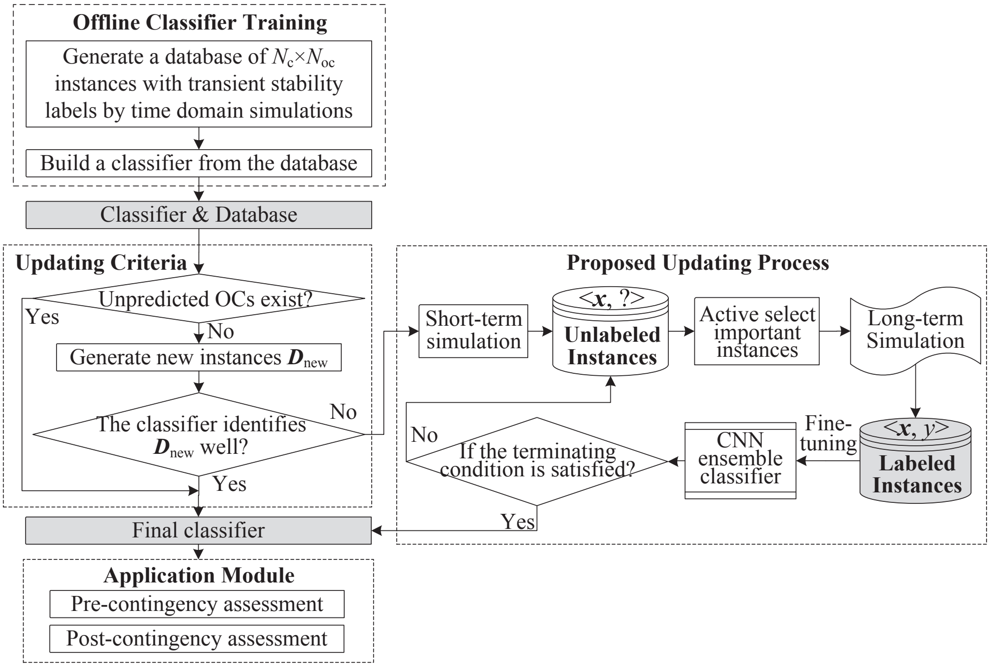
Offline Classifier Training
Generate a database of $N_c \times N_{oc}$ instances with transient stability labels by time domain simulations
Build a classifier from the database
Classifier & Database
Updating Criteria
Unpredicted OCs exist?
Yes
No
Generate new instances D_{new}
The classifier identifies D_{new} well?
No
Yes
Final classifier
Application Module
Pre-contingency assessment
Post-contingency assessment
Proposed Updating Process
Short-term simulation
<x, ?>
Unlabeled Instances
Active select important instances
Long-term Simulation
<x, y>
Labeled Instances
Fine-tuning
CNN ensemble classifier
If the terminating condition is satisfied?
No
Yes

Fig. 6. Details of the proposed scheme for transient stability prediction.

predicted using a short-term generation & load forecast and the associated unit commitment rules [18,21,42]. If the prospective OCs and anticipated contingencies are close to any of the OCs and contingencies already considered in the offline process, the classifier can be viewed as effective. When new OCs or anticipated contingencies appear or are predicted, new instances $\boldsymbol{D}_{\text{new}}$ should be generated based on the new OCs and contingencies [21]. If the prediction accuracy of the classifier for $\boldsymbol{D}_{\text{new}}$ reaches to a set value A_{set}, the classifier remains frozen until the next updating period. Otherwise, the classifier should be updated by the proposed updating scheme.

During the updating process, generally, the required number of instances considering N_{oc}' new operation conditions and N_{c}' contingencies for the next period should be obtained to update the new training dataset. The real operation data can be added as the new OCs. Moreover, the uncertainties should be considered to generate comprehensive OCs. Then the classifier is retrained by the new dataset. However, it is time-consuming for massive time-domain simulations and the classifier training especially for deep learning approaches. To reduce the computation cost, the active learning and fine-tuning techniques are used in the proposed updating strategy for transient stability prediction.

In the proposed updating scheme, the required number of unlabeled instances considering N_{oc}' new operation conditions and N_{c}' contingencies for the next period should be obtained via a short-term simulation, that is $\boldsymbol{X}_s^{\text{new}}$ where $s = 1 \ldots N_{\text{oc}}' \times N_{\text{c}}'$. N_{oc} and N_{c} are related to the scale of power systems and the time period for application. These unlabeled instances will be placed into the pre-trained or old classifier to determine which N_{new} instances are important for the updating process. Only N_{new} instances will be annotated with the target labels using long-term simulation at each iteration (The value of N_{new} is manually set). These new labeled instances ($\boldsymbol{X}_{si}^{\text{new}}$, y_{si}^{new}) will be put into the new training database, then the classifier is updated by fine-tuning the pre-trained classifier using the new training database. The aforementioned process will continue until the performance of the new classifier for $\boldsymbol{D}_{\text{new}}$ is satisfied. Then the new classifier will be used as the final classifier for the next period.

Given an unlabelled instance set $\boldsymbol{D}_u$, a labelled training set $\boldsymbol{D}_l$, a new labelled testing set $\boldsymbol{D}_{new}$, an uncertainty function f_u, and a pre-trained classifier M_0, the proposed updating algorithm is shown as follows.

Algorithm 1 Proposed Updating Scheme Integrating Active Learning and Fine-tuning Techniques

```
Given the number of new labelled instances at each iteration, $N_{\text{new}}$, and the iteration
    time $i = 0$.
While (the terminating condition is not satisfied) do:
    1. $i \leftarrow i + 1$
    2. Compute the uncertainty index, $e_{LC}$, of all the unlabelled instances.
    3. Query the label of the top $N_{\text{new}}$ instances with higher uncertainty by long-term
    simulation, $\boldsymbol{D}_{ni}$
    4. $\boldsymbol{D}_l \leftarrow \boldsymbol{D}_l \cup \boldsymbol{D}_{ni}$
    5. Obtain the new classifier $M_i$ by fine-tuning $M_{i-1}$ using $\boldsymbol{D}_l$.
    6. Go to 1 if the terminating condition is not satisfied
end while
```

One key component of this algorithm is to construct the uncertainty measure for the unlabelled instances. For the binary classification for transient stability prediction, the uncertainty measure is sufficient to determine which instances should be annotated labels. A basic uncertainty sampling strategy is to query the instance whose predicted output has the lowest confidence [32]:

$$e_{LC} = \arg\min P_z(\hat{y}\,|\boldsymbol{X}) \tag{9}$$

where $\hat{y}$ is the most likely label with the highest posterior probability in the hypothesis. This index prefers the instances with the least confidence (or highest uncertainty) in deciding their most likely class labels. For example, the output of an unknown instance $\boldsymbol{X}_1$ is $P_Z(C_1|\boldsymbol{X}_1) = 0.45$, $P_Z(C_2|\boldsymbol{X}_1) = 0.55$. Therefore the most likely label of $\boldsymbol{X}_1$ is class-2, the confidence of $\boldsymbol{X}_1$ is 0.55, and the uncertainty of $\boldsymbol{X}_1$ is 0.45. In contrast, the output of an unknown instance $\boldsymbol{X}_2$ is $P_Z(C_1|\boldsymbol{X}_2) = 0.05$, $P_Z(C_2|\boldsymbol{X}_2) = 0.95$. Although the most likely label of both $\boldsymbol{X}_1$ and $\boldsymbol{X}_2$ are class-2, the prediction confidence of $\boldsymbol{X}_2$ is 0.95 whereas $\boldsymbol{X}_1$ is 0.55. Therefore, the instance $\boldsymbol{X}_1$ with less confidence is preferred to be annotated a label in this strategy.

In the Algorithm 1, the number of epochs is selected as eight during the fine-tuning process at each iteration. The terminating condition is satisfied only if one of the following conditions is true: (1) The accuracy for $\boldsymbol{D}_{\text{new}}$ reaches to a set value A_{set}. (2) The accuracy for $\boldsymbol{D}_{\text{new}}$ cannot improve during T_{set} iterations. In the case studies, $A_{\text{set}} = 98\%$, $T_{\text{set}} = 10$.

Based on the proposed updating process, only $i \times N_{\text{new}}$ instances are annotated with the target labels using long-term simulation and added into the training database, where i is the iteration time, N_{new} is manually set. Therefore, the computational time of both the time-domain simulation and classifier training can be greatly reduced, making the proposed approach more suitable for practical application.

4.3. Application

The inputs of the CNN ensemble classifier include dynamic data. As mentioned before, these dynamic responses can be obtained from real-time measurements as well as short-term simulations [18], therefore, the CNN ensemble classifier can be applied to both the post-contingency and pre-contingency application.

For the pre-contingency application, the short-time simulation is used to prepare dynamic inputs. The transient stability of power systems under anticipated contingencies can be estimated using the generated classifier. The system security state is determined through the comprehensive results of the stability under all anticipated contingencies.

For the post-contingency application, the rotor position measure method is adopted to obtain the measurements of generator rotor angles [12], and the trajectories of electromagnetic power are calculated by the voltage magnitude and current of different generators. Therefore, these dynamic responses can be obtained from measurements and sent into the CNN ensemble classifier to rapidly predict the transient stability of power systems. Generally, the performance of classifiers with longer response time is better than the classifiers with shorter response time. The sooner the prediction is completed, the longer the time available to take countermeasures to prevent a possible collapse will be. It is hard to draw a definite conclusion about how long the best response time for any power system should be. In [43], a hierarchical scheme is proposed for transient stability prediction, the classifiers with different response times constitute the different layers to balance the rapidity and accuracy. And the hierarchical scheme can also be used for the proposed CNN ensemble classifier in this research.

On the other hand, it should be noted that the data-driven method is NOT a replacement but addition for other methods. In practical application, the data-driven method should be used combining with the time-domain simulation and other methods based on a multiple level structure in Fig. 7. On the first level, the data-driven method is responsible to rapidly predict the transient stability status of power systems under anticipated or occurred contingencies. For some cases with low prediction confidence, it is reasonable to view these cases as uncertain temporary. And these uncertain cases can be further identified by time-domain simulation or other methods.

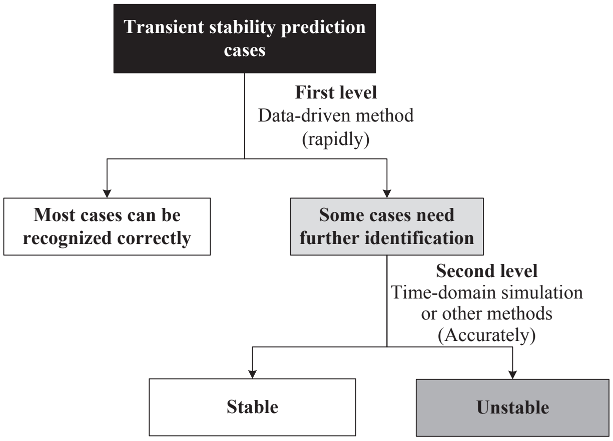
Transient stability prediction cases
First level
Data-driven method
(rapidly)
Most cases can be recognized correctly
Some cases need further identification
Second level
Time-domain simulation or other methods
(Accurately)
Stable
Unstable

Fig. 7. Application mode combining the data-driven methods and other methods.

5. Case study

5.1. Data generation

The generations and loads are randomly changed around 80–120% of standard operating point to generate a statistically sound dataset. The generation of real power, relative power, real power generation and the terminal voltage of generation at i-th operating point are based on the following equations [18]:

$$P_L^{(i)}(s) = P_{LO}^{(i)}(s) + \Delta P_{LO}^{(i)}[1 - 2 \times \varepsilon_{PL}^{(i)}(s)] \tag{10}$$

$$Q_L^{(i)}(s) = Q_{LO}^{(i)}(s) + \Delta Q_{LO}^{(i)}[1 - 2 \times \varepsilon_{QL}^{(i)}(s)] \tag{11}$$

$$P_G^{(i)}(k) = P_{GO}^{(i)}(k) + \Delta P_{GO}^{(i)}[1 - 2 \times \varepsilon_{PG}^{(i)}(k)] \tag{12}$$

$$V_G^{(i)}(k) = V_{GO}^{(i)}(k) + \Delta V_{GO}^{(i)}[1 - 2 \times \varepsilon_{VG}^{(i)}(k)] \tag{13}$$

where $\Delta P_{LO}^{(i)}$, $\Delta Q_{LO}^{(i)}$ and $\Delta P_{GO}^{(i)}$ stand for the variation range of load and generation power, $\Delta V_{GO}^{(i)} = 0.02$ means the variation range of the generator terminal voltage is ± 2%, $\varepsilon_{PL}^{(i)}(k)$, $\varepsilon_{QL}^{(i)}(k)$, $\varepsilon_{PG}^{(i)}(k)$, $\varepsilon_{VG}^{(i)}(k)$ are the random number in [0,1].

Three-phase short circuit faults at three locations (10%, 50% and 90% of the head of line) of all the transmission lines are considered. Four types of fault clearing times ranging from 6 to 12 cycles with an increment of 2 cycles (1 cycle is 0.0167 s for 60 Hz system) are assumed for all the contingencies.

To annotate the label of different operation conditions and contingencies, the time domain simulation should be conducted. The transient stability index, η, is calculated from the generator rotor angles [44]:

$$\eta = \frac{360^{o} - |\Delta\delta|_{\max}}{360^{o} + |\Delta\delta|_{\max}} \tag{14}$$

where $|\Delta\delta|_{\max}$ is the absolute value of the maximum angle of separation between any two generators after disturbance. When $\eta \geq 0$, the system is considered as stable and vice versa. Thus, the power system is considered as transiently unstable when $|\Delta\delta|_{\max} > 360^{\circ}$. It should be noted that the stability criterion is dependent on the power system characteristics [10], and different researches have used different criteria. The criterion in [18] is whether the difference between the rotor angles of any two generators exceeds 360° in the 3 s after clearing time. In [30,43,45], the criterion is 360° in the 4 s after clearing time. In [11], the criterion is 360° during 6 s simulation. In this research, the criterion for transient stability is whether the difference between the rotor angles of any two generators exceeds 360° within 4 s after the fault clearance. All the transient stability simulations are conducted using the Power System Toolbox 3.0 [46].

Two test power systems—the 10-machine 39-bus power system and the NPCC 48-machine 140-bus system—are used for the case study. The excitation systems and detailed models of synchronous generators are considered in these two power systems. The dynamic parameters of 10-machine power system can be found in [47], and the dynamic parameters of 48-machine power system are taken from the power system toolbox [46].

5.2. Evaluation indices

A useful tool for evaluating the performance of classifiers is the confusion matrix, shown in Table 3.

Table 3
Confusion matrix.

Confusion matrix	Stable (Predicted)	Unstable (Predicted)
Stable (Actual)	T_s	F_{us}
Unstable (Actual)	F_s	T_{us}

Setting N_s and N_{us} as the total number of stable and unstable instances, respectively, there are $N_s = T_s + F_{us}$ and $N_{us} = T_{us} + F_s$. Therefore, the related indices are defined as follows [48,49]:

$$\textit{Accuracy}: Acc = (T_s + T_{us})/(N_s + N_{us}) \tag{15}$$

$$\textit{Reliability}: A_{us} = T_{us}/(N_{us} + F_{us}) \tag{16}$$

$$\textit{Security}: A_s = T_s/(N_s + F_s) \tag{17}$$

$$G - mean: G = \sqrt{A_{us} \times A_s} \tag{18}$$

Accuracy is a widely used index without considering class imbalance. *Reliability* and *Security* denote the ratio of correctly identified unstable cases and stable cases, respectively. *G-mean* is a geometric mean of the *Reliability* and *Security*, evaluating the overall performance of the classifier for imbalanced data, which is the main concern in this research.

5.3. Performance of the CNN ensemble classifier

(1) Ensemble CNN Classifier vs Single CNN Classifier

To verify the effectiveness of the proposed CNN ensemble classifier, two test systems are used to generate the training data and testing data. The ratio of the test data to the training data is approximately equal to 1/4, as shown in Table 4.

Different CNN classifiers are generated using the training data with 9 cycles data (150 ms for this 60 Hz system) to predict the transient stability. Setting $W_{us} = W_s = 1$ in the loss function. Tables 5 and 6 show the performances of different classifiers for testing datasets of the 10-machine system and the 48-machine system, respectively.

Tables 5 and 6 show that the prediction errors of different CNN classifiers are different for different datasets, e.g. the CNN 1 (CNN with size 3 × 3 of the first convolution layer) performs the worst in 10-machine system but the best of the three CNN classifiers in 48-machine system. By using the ensemble method, the proposed CNN ensemble classifiers perform the best, with the highest G-mean for these two test power systems, and therefore the diverse errors are avoided.

(2) Cost Ratio Adjustment vs Without Cost Ratio Adjustment

Table 7 shows the prediction results of testing data using different cost ratios W_{us}/W_s in the loss function (6), where W_{us} and W_s are the weights of unstable and stable instances, respectively.

With the increase of cost ratios, the CNN-based ensemble classifier successfully identifies more unstable instances, whereas the number of accurately identified stable instances is reduced. Nevertheless, the performance is still satisfied due to the high G-mean and accuracy (above 98%). It can be seen that the classifier has the highest G-mean value when $W_{us}/W_s = 2$ and $W_{us}/W_s = 4$ for the 10-machine system and 48-machine system, respectively.

Having a careful check of the training data in Table 4, the ratio of stable instance number (N_s) and unstable instance number (N_{us}) is 10539/5779 ≈ 1.82 for the 10-machine system, and N_s/N_{us} = 66744/17055 ≈ 3.91 for the 48-machine system. It can be found that the best value of W_{us}/W_s is pretty close to the value of N_s/N_{us} in the training data. Therefore, it is recommended to directly use a similar value of N_s/N_{us} for W_{us}/W_s when the training data is imbalanced with less unstable cases.

Table 4
Description of the training and testing data.

Test system	Training data			Testing data		
	Total	Stable	Unstable	Total	Stable	Unstable
10-machine system	16,318	10,539	5,779	4,082	2,636	1,446
48-machine system	83,799	66,744	17,055	21,033	16,690	4,343

Table 5
Prediction results of testing data of the 10-machine system using different CNN classifiers.

Classifier	G-mean	Reliability	Security	Accuracy
CNN 1	97.90%	96.54%	99.28%	98.31%
CNN 2	98.19%	98.13%	98.25%	98.21%
CNN 3	98.45%	98.06%	98.84%	98.29%
Ensemble	98.55%	98.27%	98.84%	98.63%

Table 6
Prediction results of testing data of the 48-machine system using different CNN classifiers.

Classifier	G-mean	Reliability	Security	Accuracy
CNN 1	98.15%	97.40%	98.91%	98.60%
CNN 2	97.81%	96.45%	99.19%	98.62%
CNN 3	98.07%	97.17%	98.97%	98.60%
Ensemble	98.22%	97.28%	99.16%	98.77%

(3) Ensemble CNN Classifier vs Other Kinds of Classifiers

An additional four classifiers are generated using the same training data in Table 4 for comparison: decision tree (DT), random forest (RF) with 100 trees, and multilayer perceptron (MLP) with four hidden layers. The decision tree is the classification and regression tree based on Gini impurity. The kernel size of the four fully-connected layers in MLP are 100, 50, 10 and 2 respectively. Considering the class imbalance in the training data, the extended data [19] is used to train the DT, RF and MLP. For the 10-machine system, the unstable cases are replicated one time to obtain the extended data. For the 48-machine system, the unstable cases are replicated three times. Then the DT, MLP and RF generated by the extended data are called as the extended DT, extended MLP and extended RF, respectively. Two layers of LSTM memory blocks are employed in the LSTM layer, where each layer has 128 memory blocks [29]. The network of LSTM and CNN are trained for up to 100 epochs. The three CNNs are trained in parallel. All these methods are run on a PC with an Intel Core i7-4790 3.6-GHz processor, 16 GB of RAM and a Titan X Pascal GPU. Tables 8 and 9 show the performance of different classifiers for the testing datasets of the 10-machine system and 48-machine system, respectively.

Tables 8 and 9 show that the proposed CNN ensemble classifiers perform the best, with the highest G-mean values for these two test power systems. The order of the test time for one instance is 10^{-3} s. The memory space of the CNN ensemble classifiers for the two test system are the same because the parameter numbers are equal (Table 2). The training time of CNN ensemble classifier is a little long but still acceptable because the training process is conducted offline.

On the other hand, the training time of 48-machine system increases from 417.38 s to 2056.27 s mainly because the number of training instances increases. Fig. 8 shows the training time of the CNN ensemble classifier using different numbers of training instances.

It can be seen from Fig. 8 that, when using the same number of training instances, there are minor differences between the training time of the 10-machine system and 48-machine system because the parameter numbers are equal in Table 2. For a larger power system, therefore, the training time mainly depends on the number of instances when using the same CNN ensemble classifier with the same epochs.

(4) Effect of Noise

The input features can be provided from measurements and computations, whereas errors may be involved for practical application.

Table 7
Prediction results of testing data using different cost ratios.

W_{us}/W_s	10-machine system				48-machine system			
	Accuracy	Reliability	Security	G-mean	Accuracy	Reliability	Security	G-mean
1	98.63%	98.27%	98.84%	98.55%	98.77%	97.28%	99.16%	98.22%
2	98.58%	98.69%	98.52%	98.60%	98.75%	97.90%	98.97%	98.43%
3	98.16%	99.03%	97.69%	98.36%	98.67%	98.34%	98.75%	98.54%
4	98.16%	99.03%	97.69%	98.36%	98.52%	98.71%	98.47%	98.59%
5	98.16%	99.03%	97.69%	98.36%	98.09%	99.17%	97.81%	98.49%

More case studies are conducted to test the prediction performance considering the input errors. The errors were simulated by adding white noises following Gaussian distribution $N(0, \sigma)$ to each variable in the original testing set to generate a new testing set. The new variables x_{ij}' in the testing set is

$$x_{ij}' = x_{ij} \times (1 + \theta), \theta \sim N(0, \sigma) \quad (19)$$

The range of σ is selected from 0.01 to 0.08, the prediction results of different classifiers in Tables 8 and 9 are tested. The G-mean value of the testing data are presented in Fig. 9. It can be found that the proposed CNN ensemble classifier has the best performance under the noise condition.

(5) Performance of the CNN Ensemble Classifiers with Different Response Time

For post-contingency application, the total prediction time of the CNN ensemble classifier is related to the response time of inputs, computation time of CNN ensemble classifier and the latency. The latency is unavoidable for any methods. The computation time for one instance after the inputs obtained is 0.004 s. Therefore, the response time is a key aspect for the total prediction time. The performance of the CNN ensemble classifiers using the features with different response times is tested, shown in Fig. 10.

It can be seen that the performance of CNN ensemble classifier is better when using a longer response time. To balance the rapidity and accuracy of transient stability prediction, the hierarchical scheme in [43] can be used for the CNN ensemble classifier.

Take the CNN ensemble classifier with 0.05 s response time as an example, the instability occurrence time histogram of the total testing unstable instances, the detected and undetected unstable instances are compared in Fig. 11.

Fig. 11(a) shows the instability occurrence time histogram of the total testing unstable instances. Fig. 11(b) shows that the CNN ensemble classifier can even detect some cases that instability occur after 3 s after the fault clearance. In Fig. 11(c), the instability occurrence times of the most of the undetected unstable instances are longer than 1 s. It can be found that the proposed CNN ensemble classifier can rapidly detect some instabilities. The average of the instability occurrence time in all the detected unstable instances is 0.8242 s, the response time is 0.05 s, the computation time of CNN is 0.004 s. Therefore, the average preemptive time of the proposed method before instability occurs is 0.7702 s regardless of the latency.

(6) Comparisons among different classifiers with different input features

In the literatures, the voltage-related variables are always used as the inputs because these variables can be obtained directly by phasor measurement units (PMUs). These features can also be used for the proposed CNN ensemble classifier. In this section, the voltage magnetic and phase angles of all the generator buses over the time span of 150 ms after fault clearing are used as the inputs. Then the extended DT, MLP, RF, LSTM and CNN ensemble classifiers are obtained using the same training data in Section 5.3 (3). The prediction results of different classifiers for the test data in 10-machine system are shown in Table 10. It can be seen from Table 10 that, when using the voltage variables as the inputs, the ensemble CNN classifier still perform the best with the highest G-mean value.

In [50], 34 features are extracted from the original trajectories. These features are also used to train a SVM from the same training data in Table 4 for comparison. Besides, the extended SVM is trained from the extended data. The response time is 150 ms after the fault clearing. The parameters of SVM are search by a cross validation with grid-search process. Table 11 shows the performances of different classifiers for testing datasets of the 10-machine system.

It should be noted that the data in this research and Ref. [50] are different. Although the SVM classifier has good performance than the other shallow models, the proposed CNN ensemble classifier (in Table 8) still possesses the best performance with the highest G-mean.

(7) Performance of the CNN ensemble classifier using the features of part of generators

For the post-contingency application, the inputs can only be obtained from real-time measurements. Considering the PMU locations, only the measurements of some generators can be obtained. Therefore, the prediction performance of the CNN ensemble classifier using the information of parts of generators should be considered.

To verify the effectiveness of the proposed approach, the CNN ensemble classifier is retrained only using the features of part of generators. When the features of any one generator are removed from the original inputs, the G-mean and accuracy of the CNN ensemble classifier for the test data in 10-machine system are shown in Fig. 12.

When the features of multiple generators are removed from the original inputs, the situations are more complex because of the randomness. For simplicity, only the situations when the generators' features are removed according to the descending order of the G-mean

Table 8
Prediction results of testing data of the 10-machine system using different classifiers.

Classifier	Training time	Test time (one instance)	Memory	G-mean	Reliability	Security	Accuracy
Extended CART	19.28 s	0.001 s	49 K	95.68%	94.67%	96.70%	95.98%
Extended MLP	10.80 s	0.001 s	1590 K	97.37%	97.37%	97.38%	97.38%
Extended RF	57.68 s	0.009 s	4929 K	97.81%	97.86%	97.76%	97.80%
LSTM, $W_{us}/W_s = 2$	2220.20 s	0.022 s	4194 K	98.20%	98.34%	98.07%	98.16%
Ensemble CNN, $W_{us}/W_s = 2$	417.38 s	0.004 s	3489 K	98.60%	98.69%	98.52%	98.58%

Table 9
Prediction results of testing data of the 48-machine system using different classifiers.

Classifier	Training time	Test time (one instance)	Memory	G-mean	Reliability	Security	Accuracy
Extended CART	858.01 s	0.001 s	149 K	95.96%	93.32%	98.67%	97.54%
Extended MLP	527.98 s	0.002 s	6934 K	97.55%	98.69%	96.42%	96.89%
Extended RF	1047.52 s	0.009 s	18862 K	98.25%	97.61%	98.89%	98.63%
LSTM, $W_{us}/W_s = 4$	11680.91 s	0.022 s	5334 K	98.06%	98.13%	97.99%	98.08%
Ensemble CNN, $W_{us}/W_s = 4$	2056.27 s	0.004 s	3489 K	98.59%	98.71%	98.47%	98.52%

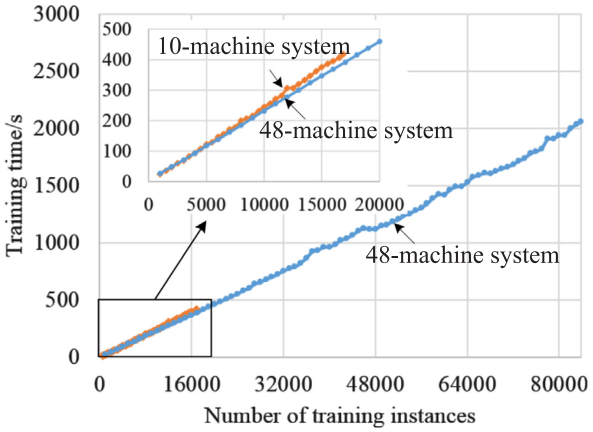

Fig. 8. The training time using different numbers of training instances.

value in Fig. 12. Ten generator sets are shown in Table 12.

The prediction results of the CNN ensemble classifier using different generator sets are shown in Fig. 13.

Fig. 13 shows that the more generators are considered as the input features, the better the CNN ensemble classifier performs. Besides, the prediction results show that the proposed approach is effective (higher than 97%) when only using the measurements of three generators.

5.4. Performance of the CNN ensemble classifier considering the variation in operation conditions

In Section 5.3, because the training data and testing data are randomly selected from a total dataset, the operating conditions in testing dataset may exist in the training dataset. However, in practical application, the operating conditions cannot be the same as those of the offline simulation scenarios. Therefore, it is more reasonable to verify the generalizability of the proposed classifier under different generations, loads and network configurations.

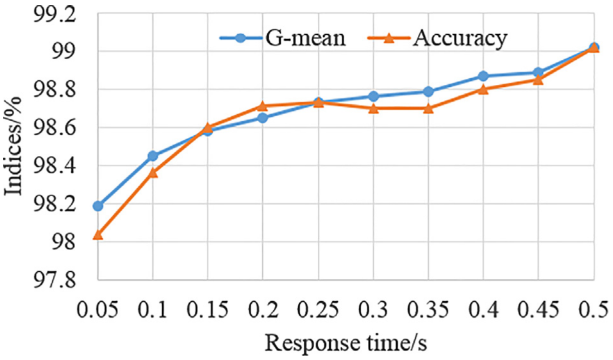

Fig. 10. Prediction results of the CNN ensemble classifier with different response time of 10-machine system.

(1) New England 10-machine 39-bus system

Two new untrained datasets are generated to verify the generalizability of the proposed classifier under different scenarios. Details of the power flow and network configuration are shown in Table 13.

For the new test data 1, the new power flows within a similar range can be used to simulate the normal variation in operating situation. The new test data 2 is used to simulate the major variations. Fig. 14 shows the prediction results of different classifiers for these two new datasets.

Fig. 14(a) shows that the proposed CNN ensemble classifier performs the best under the normal variation in power flow because it has the highest G-mean for this unbalanced testing set. Furthermore, the accuracy of the proposed CNN ensemble classifier is still up to 97.7%. Therefore, the proposed method can cope with the normal changes of operation conditions.

When the power flow and network configuration change substantially, the performance of all the classifiers is reduced notably (Fig. 14(b)). The CNN-based ensemble classifier must adjust itself to make it suitable to the new operating condition. The performance of the proposed updating scheme will be validated in Section 5.5.

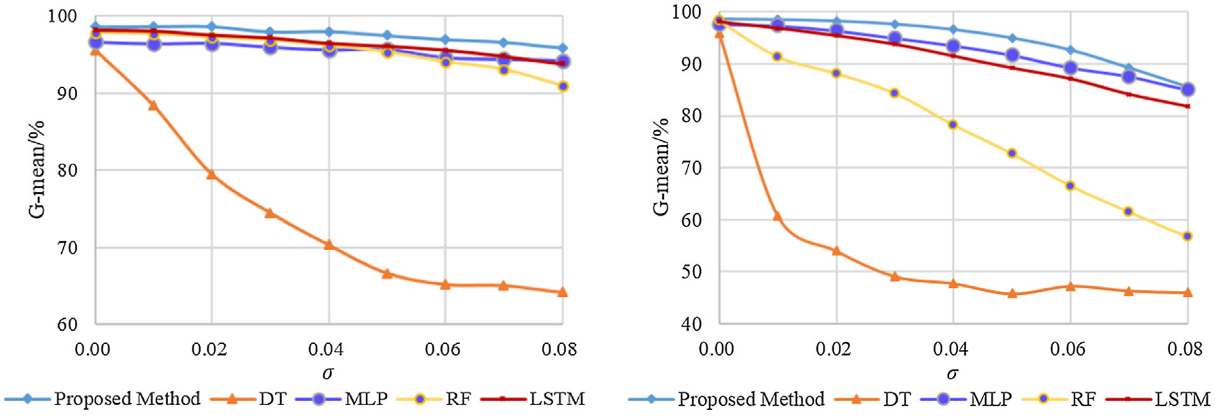

(a) 10-machine system

(b) 48-machine system

Fig. 9. Comparison of different methods considering the effect of noise.

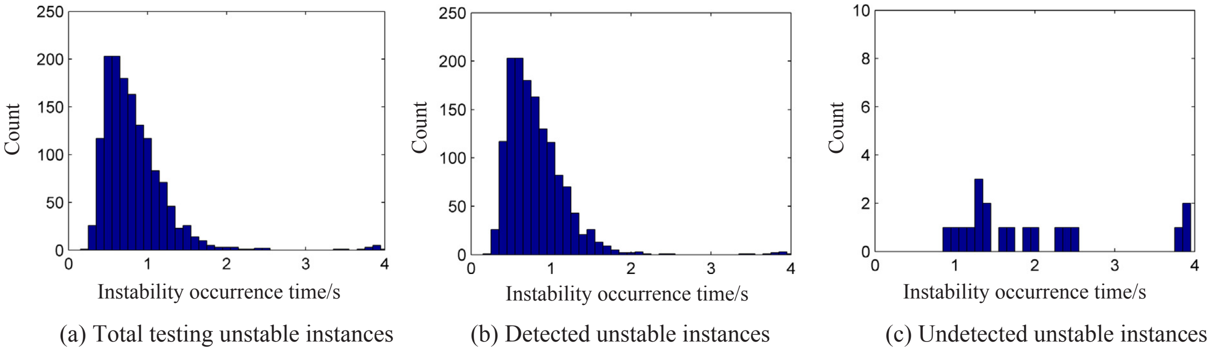

(a) Total testing unstable instances (b) Detected unstable instances (c) Undetected unstable instances

Fig. 11. Instability occurrence time histogram of unstable instances.

Table 10
Prediction results of testing data of the 10-machine system using the voltage variables as the inputs.

Classifier	G-mean	Reliability	Security	Accuracy
Extended CART	92.24%	91.70%	92.79%	92.41%
Extended MLP	94.09%	95.37%	92.83%	93.73%
Extended RF	96.43%	96.27%	96.59%	96.47%
LSTM, $W_{us}/W_s = 2$	96.41%	95.71%	97.12%	96.62%
Ensemble CNN, $W_{us}/W_s = 2$	97.51%	98.20%	96.81%	97.31%

Table 11
Prediction results of testing data of the 10-machine system using SVM and 34 features in [50].

Classifier	G-mean	Reliability	Security	Accuracy
SVM	97.82%	97.51%	98.14%	97.92%
Extended SVM	97.90%	98.20%	97.61%	97.82%

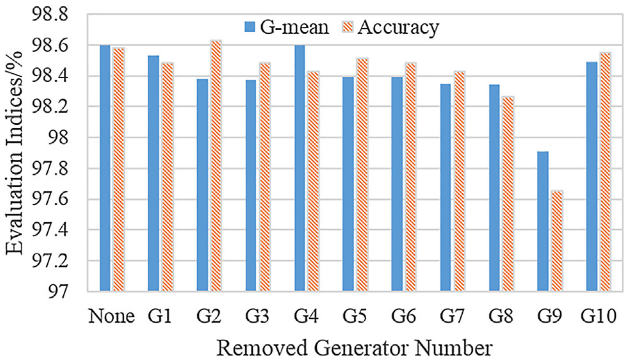

Fig. 12. Prediction results when removing one generator's information from the feature set.

Table 12
Generator sets when removing multiple generators' information.

Generator set	Descriptions
1	{G1,G2,G3,G4,G5,G6,G7,G8,G9,G10}
2	{G1,G2,G3,G5,G6,G7,G8,G9,G10}
3	{G2,G3,G5,G6,G7,G8,G9,G10}
4	{G2,G3,G5,G6,G7,G8,G9}
5	{G2,G3,G6,G7,G8,G9}
6	{G2,G3,G7,G8,G9}
7	{G3,G7,G8,G9}
8	{G7,G8,G9}
9	{G8,G9}
10	{G9}

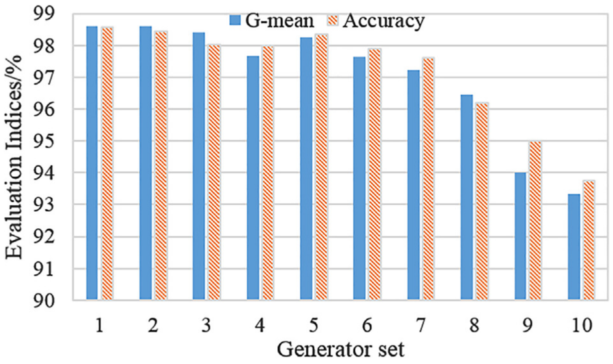

Fig. 13. Prediction results of CNN ensemble classifier when using different generator sets.

(2) NPCC 48-machine 140-bus system

The variations in operating conditions are also considered in the larger 48-machine system. Details of the new untrained data are shown in Table 14. The prediction results of different classifiers to these new test datasets are shown in Fig. 15.

Fig. 15(a) shows that the proposed CNN-based ensemble classifier performs the best because it has the highest G-mean for these unbalanced testing sets. However, the performance of all the classifiers is reduced greatly in Fig. 15(b) when the operation conditions change substantially. Therefore, the classifier should be updated using new instances.

5.5. Performance of the proposed updating scheme integrating active learning and fine-tuning

According to the previous simulation results, the performance of the classifier will decrease when the operating condition of the power system changes greatly. In fact, these variations can be predicted by generation and load forecasting, dispatching, scheduled maintenance, etc. Based on this information, the classifier should be updated in a limited time. A fast updating scheme can make sure the practical application. To verify the performance of the proposed updating strategy, the comprehensive simulation will be conducted on the two test systems.

(1) New England 10-machine 39-bus system

An additional 11,832 instances are randomly generated using similar configurations as used in testing set 2 (Table 13) to construct the new updating dataset. The power flow of the updating and test datasets are completely different because of the stochastic property in Eqs. (10)–(13). Three different learning strategies are considered to compare the effectiveness of the proposed updating strategy using the same

Table 13
Different scenarios of new testing data of 10-machine system.

	Power Flow	Network Configuration	Stable	Unstable
New Test Data 1	Randomly generated from 80 to 120% of standard power flow (different from training data)	All the lines are in service	2,576	1,504
New Test Data 2	Randomly generated from 115 to 135% of standard power flow	An static var compensator (SVC) and a thyristor controlled series compensator (TCSC) are added at bus 21 and line 2–25, respectively	1,510	2,570

number of training instances.

Scheme 1: Fine-tuning the pre-trained classifier based on the instances selected by the active learning strategies.
Scheme 2: Retraining a new classifier based on the instances selected by the active learning strategies.
Scheme 3: Retraining a new classifier based on the instances randomly selected.

The number of selected labelled instances are 204, 408, 612, 816, … , 11,832 ($N_{\text{new}} = 204$ in the Algorithm 1). Since the new test data 2 in Table 13 contains more unstable instances, the values of W_{us} and W_{s} are set as 1 during the updating process. The performances of classifiers obtained from different learning strategies are shown in Fig. 16.

Fig. 16(a) shows that the accuracies of the training set (including unlabelled instances) of Scheme 1 and 2 are higher than that of Scheme 3, therefore, active selection strategy can select representative instances from unlabelled data. Fig. 16(b) shows that the prediction accuracy of Scheme 1 using the classifier trained by only 816 labelled instances is 98.01%. Therefore, only 816 labeled instances are needed to be obtained by long-term simulation. In contrast, Scheme 2 and Scheme 3 cannot achieve this level of performance even when using all the instances. As a result, the proposed method can obtain an accurate classifier using fewer instances, thereby dramatically reducing the computational time, including the time for time-domain simulation and classifier training.

To investigate the distribution of the instances selected by three schemes, the t-distributed stochastic neighbour embedding (T-SNE) [51] is used to provide the visualization of the top 816 instances selected by different schemes, as shown in Fig. 17. The high-dimensional features of the top 816 instances selected by different schemes are reduced into two dimensions by T-SNE. There are some overlapping areas in the visualization results. The overlapping is the main reason for classification difficulties, and the instances in overlapping area are more important to obtain the new classifier. Compared with the Scheme 2 and Scheme 3, shown in Fig. 17, Scheme 1 can select more instances in the overlapping areas, allowing the proposed method to obtain an accurate classifier with fewer training instances.

Table 15 shows the detailed results of different schemes using 816 instances and those of Scheme 3 using all 11,832 instances.

Table 15 shows that the accuracy, reliability, security and G-mean of Scheme 1 are all the highest. Most importantly, the total computation time T_{total} of Scheme 1 (including the selection of important instances, training time using different numbers of instances during the iteration in algorithm 1) is satisfied for practical application. The training time of Scheme 2 is longer than that of Scheme 3 because the active learning should select important instances and train multiple classifiers using different numbers of instances. The fine-tuning technique enables the total training time to be dramatically reduced, making the proposed method quite suitable for online updating. Moreover, parallel computation techniques can be used with the proposed ensemble classifier to further reduce the training time.

On the other hand, data generation is a very time-consuming step in the classifier updating process. To obtain an instance with label, the time-domain simulation should be conducted. However, in the proposed approach, only the selected instances are needed to annotate a label (shown in Fig. 18). Therefore, the computation time of time domain simulation can be significantly reduced, which makes the proposed approach more suitable for practical application.

(2) NPCC 48-machine 140-bus system

An additional 74,520 instances are randomly generated with the same configuration as in the new testing set 2 in Table 14. The fast updating process described in Section 4.2 is used to obtain the new classifier using these new instances. Three different learning strategies in Section 5.5 (1) are considered to compare the effectiveness. Since the new test data 2 in Table 14 contains less unstable instances, setting $W_{\text{us}} = 3$ and $W_{\text{s}} = 1$ during the updating process. The performances of classifiers obtained using different learning strategies and different numbers of labelled instances are shown in Fig. 19.

Fig. 19(b) shows that the accuracy of the classifier on the test data is up to 98% when using only 2070 (2.78%) labelled training instances. In contrast, the performances of Scheme 2 and 3 are not satisfactory. Therefore, the proposed strategy can obtain an accurate classifier using fewer labelled instances with a shorter computational time.

Table 16 shows that detailed results of different schemes using 2070

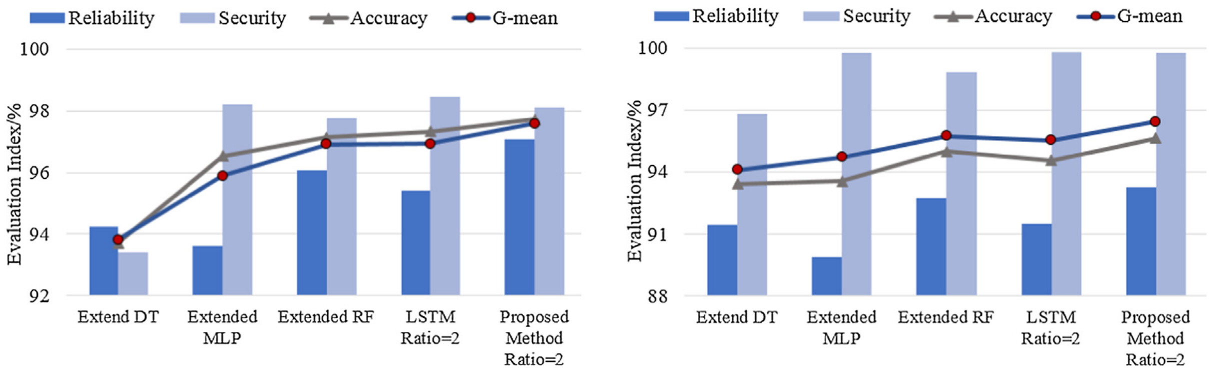

(a) New Test Data 1 (b) New Test Data 2

Fig. 14. Prediction accuracy of the new testing data in Table 13 using different classifiers.

Table 14
Different scenarios of new testing data of 48-machine system.

	Power flow	Network configuration	Stable	Unstable
New Test Data 1	Randomly generated from 80 to 120% of standard power flow (different from training data)	All the lines are in service	17,354	2,615
New Test Data 2	Randomly generated from 115 to 135% of standard power flow	Line 124–127 is out of service	14,005	5,867

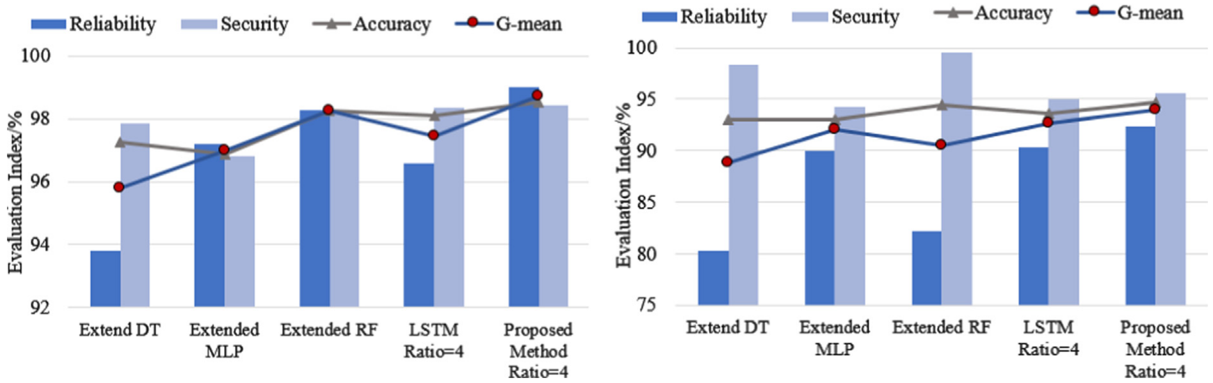

(a) New Test Data 1 (b) New Test Data 2

Fig. 15. Prediction accuracy of the new testing data in Table 14 using different classifiers.

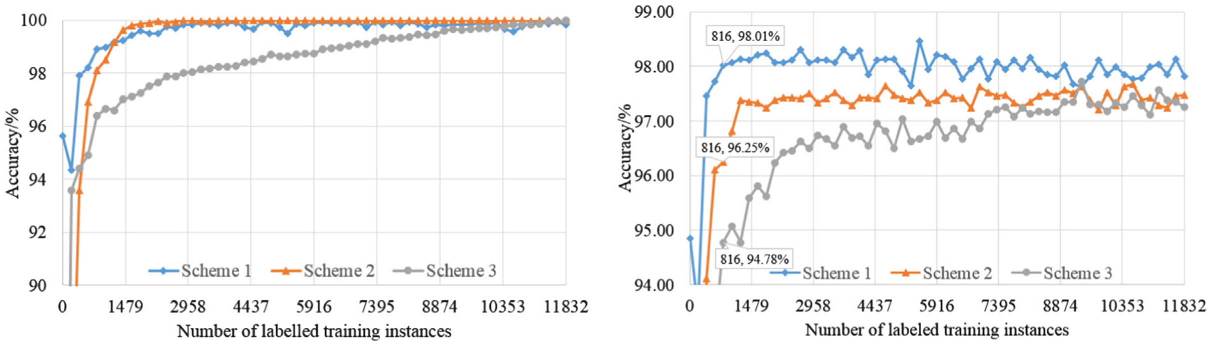

(a) Accuracy of the new training data with 11832 instances (b) Accuracy of the new test data 2 with 4080 instances (Table 13)

Fig. 16. Comparison of different methods of 10-machine system.

instances and Scheme 3 using all the 74,520 instances.

Table 16 reveals that the performance of Scheme 1 is the best, exhibiting the shorter total computation time and best evaluation index. Therefore, the proposed method is highly suitable for online application.

5.6. Discussions

(1) Selection of the input features

The reasonability of the input features has a great influence on the performance of a transient stability classifier [43]. It seems that the input features for transient stability prediction are always different in different studies. There is not a universal feature set for transient

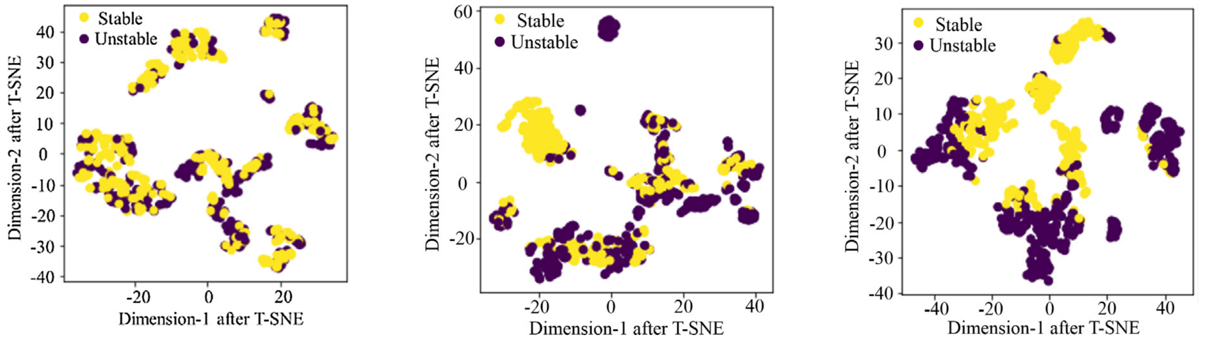

(a) 816 instances selected by Scheme 1 (b) 816 instances selected by Scheme 2 (c) 816 instances selected by Scheme 3

Fig. 17. Visualization of the selected instances by different methods.

Table 15
Prediction results of different schemes for new test data 2 in Table 13 with 4080 instances.

	N_{select}	T_{total}	G-mean	Accuracy	Reliability	Security
Scheme 1	816	21.87 s	98.01%	98.01%	98.01%	98.02%
Scheme 2	816	101.95 s	96.16%	96.25%	96.50%	95.83%
Scheme 3	816	46.37 s	94.53%	94.78%	95.49%	93.58%
Scheme 3	11,832	508.53 s	97.15%	97.25%	97.55%	96.76%

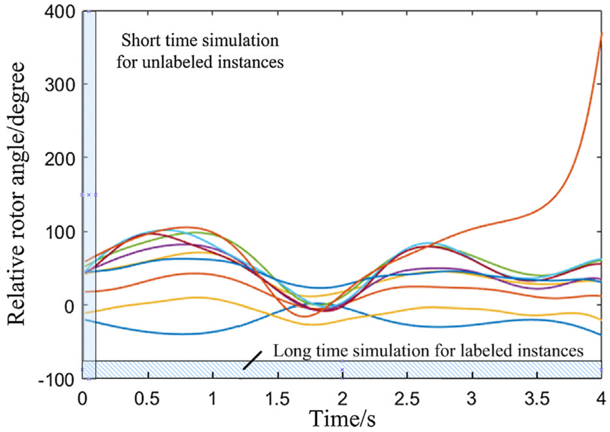

Fig. 18. Time-domain simulation result.

stability prediction. And it is hard to say that any features can always perform the best in any cases.

In practical, the selection of input features should consider the locations of measurement units. On the other hand, some variables have strong correlation with the transient stability status. If the important measurements cannot be obtained, the prediction performance will reduce significantly. Therefore, new measurement units should be installed at new locations. It can be said that the selection of input features and the location of measurement units interact each other.

Moreover, the input features are not fixed as the development of science and technology. Some variables may become measurable with the development of measurement technology. These variables should be added as the input features. On the other hand, when new progress has been achieved in the mechanism analysis of transient stability, new features should be utilized as the inputs for the data-driven methods.

(2) Considering new contingencies

For the pre-contingency application, only the credible contingencies are taken into consideration for the sake of economy. For the post-contingency application, whereas, the number of possible disturbances is infinite. Therefore, the generated classifier should possess good generalization for different contingencies. To obtain a CNN ensemble classifier with good performance under different contingencies, a comprehensive dataset should be obtained during the training process. Because the post-fault responses carry information about the influence of the faults on the power system, the generated classifier may have generalization with respect to similar contingencies. On the other hand, some contingencies can be predicted by the information of weather, equipment monitoring, forest fire prevention information, etc. Based on the new dataset considering new contingences, the CNN ensemble classifier can be updated to have good performance considering these new contingencies.

Table 16
Prediction results of different schemes for new test data 2 in Table 14 with 19,832 instances.

	N_{select}	T_{total}	G-mean	Accuracy	Reliability	Security
Scheme 1	2070	62.19 s	97.76%	98.02%	97.11%	98.42%
Scheme 2	2070	252.94 s	95.28%	96.00%	93.53%	97.06%
Scheme 3	2070	61.27 s	93.25%	94.92%	89.35%	97.32%
Scheme 3	74,520	2043.33 s	96.47%	97.16%	94.73%	98.21%

(3) Effect of stability criterion

In this research, the transient stability criterion is whether the difference between any two generator rotor angles exceeds 360° with 4 s after the fault clearance. It is reasonable because the time frame of interest in transient stability studies is usually 3–5 s [2]. However, the power system may lose the synchronous through multi swings after a longer time period. Under this condition, the criterion with shorter time period will label those multi-swing unstable instances as stable.

Different from the model-based methods start from the model solving or theoretical analysis, the data-driven method is learning from massive data. When the criterion considers longer time of period, the criterion can be reflected on the label and then learned by the data-driven method. To verify this viewpoint, case studies are conducted on the 10-machine system using 10 s criterion, and the results still show that the proposed CNN ensemble classifier performs the best among the compared methods and some multi-swing instabilities can be detected. However, similar to the results in Fig. 11, some unstable instances with longer instability occurrence time cannot be detected with shorter response time. To balance the rapidity and accuracy, the hierarchical scheme in [43] should be used.

(4) Considering different types of stability problems

The power system stability status should be determined by comprehensive consideration of different kinds of stability. In practical

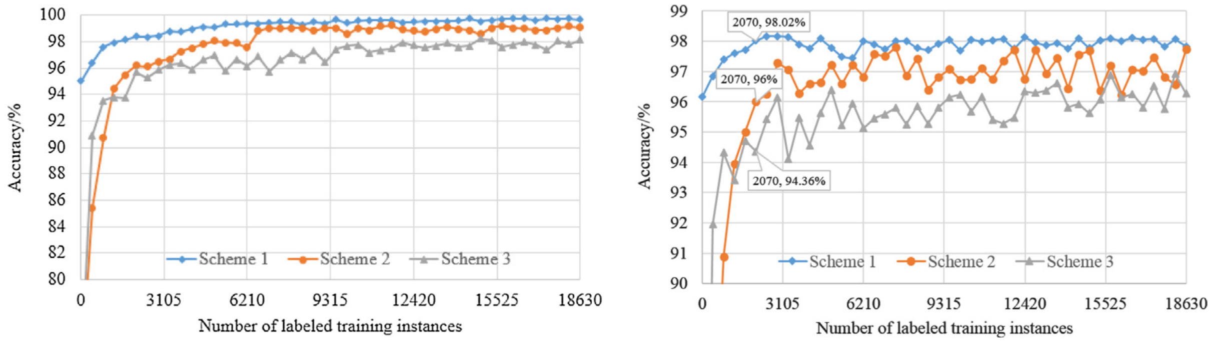

(a) Accuracy of the new training data with 74520 instances

(b) Accuracy of the new test data 2 with 19832 instances (Table 14)

Fig. 19. Comparison of different methods of 48-machine system.

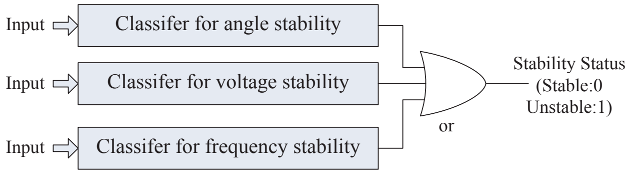
Input
Classifer for angle stability
Input
Classifer for voltage stability
Input
Classifer for frequency stability
or
Stability Status
(Stable:0
Unstable:1)

Fig. 20. Implementation of multiple classifiers considering different types of stability problems.

application, different classifiers should be trained for different kinds of stabilities, and new features and indices [52] should be considered for different stabilities. If any one of the classifiers predicted the system to be unstable, the system is considered as unstable. Therefore, the outputs of the three classifiers were combined using an OR logic, shown in Fig. 20.

The stability criterion in this research can describe the instability phenomenon, but this criterion cannot reveal the instability mechanism. In practical application, for example, the voltage and rotor angle instability always intertwined. When the power systems show several instability characteristics, addition method such as [53] should be used to recognize the dominant instability mechanism.

6. Conclusions

This paper presents a CNN-based ensemble classifier and its fast updating scheme for transient stability prediction. Through comprehensive comparisons among different methods of two test power systems, the following conclusions can be drawn:

(1) The proposed CNN-based ensemble classifier can process multi-dimensional data directly and provide accurate prediction even under the measurement errors. For unbalanced data with fewer unstable instances, the reliability (accuracy of unstable instances) of the proposed classifier can be improved by improving the cost weighting of the unstable instances.
(2) When the operating conditions change substantially, the proposed updating method can obtain an accurate classifier using only a few labelled instances. The computational time of both the time-domain simulation and classifier training can be greatly reduced, making the proposed method more suitable for online application.

Acknowledgment

The authors gratefully acknowledge the financial supports from the National Key R&D Program of China (2018YFB0904500), the China Postdoctoral Science Foundation Funded Project (2018M630156), the National Natural Science Foundation of China (51577009), and the support of NVIDIA Corporation with the donation of the Titan X Pascal GPU used for this research.

References

[1] Liao X, Liu K, Niu H, Jun L, Yuye L, Liang Q. An interval Taylor-based method for transient stability assessment of power systems with uncertainties. Int J Electr Power Energy Syst 2018;98:108–17.
[2] Kundur P, Paserba J, Ajjarapu V, Andersson G, Bose A, Canizares C, et al. Definition and classification of power system stability. IEEE Trans Power Syst 2004;19(3):1387–401.
[3] Liu CW, Thorp J. Application of synchronised phasor measurements to real-time transient stability prediction. IEE Proc Gener Transm Distrib 1995;142(4):355–60.
[4] Chiang Hsiao-dong, Chu Chia-chi, Cauley Gerry. Direct stability analysis of electric power systems using energy functions: theory, application, and perspective. Proc IEEE 1995;83(11):1497–529.
[5] Xue Y, Van Cutsem TH, Ribbens –Pavella M. A simple direct method for fast transient stability assessment of large power systems. IEEE Trans Power Syst 1988;3(2):400–12.
[6] Jahromi Mehdi Zareian, Kouhsari Shahram Montaser. A novel recursive approach for real-time transient stability assessment based on corrected kinetic energy. Appl Soft Comput 2016;48(November):660–71.
[7] Hu J, Vasilakos AV. Energy big data analytics and security: challenges and opportunities. IEEE Trans Smart Grid 2016;7(5):2423–36.
[8] Chen K, He Z, Wang SX, Hu J, Li L, He J. Learning-based data analytics: moving towards transparent power grids. CSEE J Power Energy Syst 2018;4(1):67–82.
[9] Long H, Zhang Z, Sun MX, et al. The data-driven schedule of wind farm power generations and required reserves. Energy 2018;149.
[10] Amjady N, Mahedi SF. Transient stability prediction by a hybrid intelligent system. IEEE Trans Power Syst 2007;22(3):1275–83.
[11] Guo T, Milanović JV. Probabilistic framework for assessing the accuracy of data mining tool for online prediction of transient stability. IEEE Trans Power Syst 2014;29(1):377–84.
[12] Guo T, Milanović JV. Online identification of power system dynamic signature using PMU measurements and data mining. IEEE Trans Power Syst 2016;31(3):1760–8.
[13] Aghamohammadi MR, Abedi M. DT based intelligent predictor for out of step condition of generator by using PMU data. Int J Electr Power Energy Syst 2018;99:95–106.
[14] Rajapakse AD, Gomez FR, Nanayakkara K, Crossley PA, Terzija VV. Rotor angle instability prediction using post-disturbance voltage trajectories. IEEE Trans Power Syst 2010;25(2):947–56.
[15] Gomez FR, Rajapakse AD, Annakkage UD, Fernando IT. Support vector machine-based algorithm for post-fault transient stability status prediction using synchronized measurements. IEEE Trans Power Syst 2011;26(3):1474–83.
[16] Li M, Pal A, Phadke AG, Thorp JS. Transient stability prediction based on apparent impedance trajectory recorded by PMUs. Int J Electr Power Energy Syst 2014;54(1):498–504.
[17] You D, Wang K, Ye L, et al. Transient stability assessment of power system using support vector machine with generator combinatorial trajectories inputs. Int J Electr Power Energy Syst 2013;44(1):318–25.
[18] Geeganage Janath, Annakkage UD, Weekes Tony, Archer Brian A. Application of energy-based power system features for dynamic security assessment. IEEE Trans Power Syst 2015;30(4):1957–65.
[19] Kamwa I, Samantaray SR, Joos G. Catastrophe predictors from ensemble decision-tree learning of wide-area severity indices. IEEE Trans Smart Grid 2010;1(2):144–58.
[20] Cepeda JC, Rueda JL, Colomé DG, et al. Data-mining-based approach for predicting the power system post-contingency dynamic vulnerability status. Int Trans Electr Energy Syst 2015;25(10):2515–46.
[21] Sun K, Likhate S, Vittal V, et al. An online dynamic security assessment scheme using phasor measurements and decision trees. IEEE Trans Power Syst 2007;22(4):1935–43.
[22] Cepeda JC, Rueda JL, Colomé DG, et al. Real-time transient stability assessment based on centre-of-inertia estimation from phasor measurement unit records. IET Gener Transm Distrib 2014;8(8):1363–76.
[23] Maggiori E, Tarabalka Y, Charpiat G, Alliez P. Convolutional neural networks for large-scale remote-sensing image classification. IEEE Trans Geosci Rem Sens 2017;55(2):645–57.
[24] Zhou Z, Shin J, Zhang L, Gurudu S, Gotway M, Liang J. Fine-tuning convolutional neural networks for biomedical image analysis: actively and incrementally. IEEE conference on computer vision and pattern recognition. IEEE Computer Society; 2017. p. 4761–72.
[25] Zhang W, Peng G, Li C, Chen Y, Zhang Z. A new deep learning model for fault diagnosis with good anti-noise and domain adaptation ability on raw vibration signals. Sensors 2017;17(2):425.
[26] Nguyen VN, Jenssen R, Roverso D. Automatic autonomous vision-based power line inspection: a review of current status and the potential role of deep learning. Int J Electr Power Energy Syst 2018;99:107–20.
[27] Hu Z, He T, Zeng Y, Luo X, Wang J, Huang S, et al. Fast image recognition of transmission tower based on big data. Prot Control Modern Power Syst 2018;3(15):1–10.
[28] Wang L, Zhang Z, Chen J. Short-term electricity price forecasting with stacked denoising autoencoders. IEEE Trans Power Syst 2017;32(4):2673–81.
[29] Yu JJQ, Hill DJ, Lam AYS, et al. Intelligent time-adaptive transient stability assessment system. IEEE Trans Power Syst 2018;33(1):1049–58.
[30] Zhou Y, Wu J, Ji L, Yu Z, Hao L. Transient stability preventive control of power systems using chaotic particle swarm optimization combined with two-stage support vector machine. Electr Power Syst Res 2018;155:111–20.
[31] Krizhevsky A, Sutskever I, Hinton GE. ImageNet classification with deep convolutional neural networks. International conference on neural information processing systems. Curran Associates Inc.; 2012. p. 1097–105.
[32] Settles B. Active learning: synthesis lectures on artificial intelligence and machine. Learning 2012;6(1):1–114.
[33] Fu Y, Zhu X, Li B. A survey on instance selection for active learning. Knowl Inf Syst 2013;35(2):249–83.
[34] Yixing Ni, Shousun Cheng, Baolin Zhang. Theory and analysis of the dynamic power system. Beijing: Tsinghua University Press; 2002. p. 136.
[35] Bishop CM. Neural networks for pattern recognition, London. U.K.: Oxford Univ. Press; 1995.
[36] Kingma DP, Adam BaJ. A method for stochastic optimization. Comput Sci 2014.
[37] He K, Zhang X, Ren S, Sun J. Deep residual learning for image recognition. IEEE Comput Soc 2016:770–8.
[38] Simonyan K, Zisserman A. Very deep convolutional networks for large-scale image recognition. Comput Sci 2014.
[39] Han J, Kamber M, Pei J. Data Ming: Concept and Techniques. 3rd ed. Amsterdam, The Netherlands: Elsevier; 2012. p. 363–85.
[40] Hinton GE, Srivastava N, Krizhevsky A, Sutskever I, Salakhutdinov RR. Improving

neural networks by preventing co-adaptation of feature detectors. Comput Sci 2012;3(4):212–23.

[41] Srivastava N, Hinton G, Krizhevsky A, Sutskever I, Salakhutdinov R. Dropout: a simple way to prevent neural networks from overfitting. J Mach Learn Res 2014;15(1):1929–58.

[42] Jiang Y, Long H, Zhang Z, Song Z. Day-ahead prediction of bi-hourly solar radiance with a markov switch approach. IEEE Trans Sustain Energy 2017;8(4):1536–47.

[43] Zhou Y, Wu J, Yu Z, Ji L, Hao L. A hierarchical method for transient stability prediction of power systems using the confidence of a svm-based ensemble classifier. Energies 2016;9(10):778.

[44] Pavella M, Ernst D, Vega DR. Transient stability of power systems: a unified approach to assessment and control. Norwell, MA, USA: Kluwer; 2000.

[45] Rovnyak S, Kretsinger S, Thorp J, et al. Decision trees for real-time transient stability prediction. IEEE Trans Power Syst 1994;9(3):1417–26.

[46] Chow JH, Cheung KWA. toolbox for power system dynamics and control engineering education and research. IEEE Trans Power System 1992;7:1559–64.

[47] Zhou Y. Transient stability analysis and preventive control of power systems based on data mining technique. Beijing: Beijing Jiaotong University; 2017. p. 136–7.

[48] Kamwa I, Samantaray SR, Joós G. On the accuracy versus transparency trade-off of data-mining models for fast-response PMU-based catastrophe predictors. IEEE Trans Smart Grid 2012;3:152–61.

[49] Zhu L, Lu C, Dong ZY, Hong C. Imbalance learning machine based power system short-term voltage stability assessment. IEEE Trans Ind Inf 2017;13(5):2533–43.

[50] Zhou Yanzhen, Sun Hongbin, Guo Qinglai, Xu Bo, Wu Junyong, Hao Liangliang. Data driven method for transient stability prediction of power systems considering incomplete measurements. IEEE conference on energy internet and energy system integration (EI2), 26-28 Nov. 2017, Beijing China. 2017.

[51] Van DML, Hinton G, Maaten LVD. Visualizing data using t-SNE. J Mach Learn Res 2017;9(2605):2579–605.

[52] Ravikumar Gelli. Shrikrishna A KhapardeTaxonomy of PMU data based catastrophic indicators for power system stability assessment. IEEE Syst J 2018;12(1):452–64.

[53] Wu W, Tang Y, He J, Lin W. The recognition of principal mode between rotor angle instability and transient voltage instability. Proc CSEE 2014;34(31):5610–7.